ACS OMEGA

Open Access

http://pubs.acs.org/journal/acsodf

Article

Geometric and Hydrophilic Effects of Oxirane Compounds with a Four-Carbon Backbone on Clathrate Hydrate Formation

Jiwoong Seol*

Cite This: *ACS Omega* 2023, 8, 43920−43929

Read Online

ACCESS | Metrics & More | Article Recommendations | Supporting Information

ABSTRACT: The physicochemical properties of clathrate hydrates are influenced by the chemical nature and three-dimensional (3D) geometry of the added molecules. This study investigates the effects of five oxirane compounds: *cis*-2,3-epoxybutane (*c*23EB), *trans*-2,3-epoxybutane (*t*23EB), 1,2-epoxybutane (12EB), 1,2,3,4-diepoxybutane (DEB), and 3,3-dimethyleoxybutane (33DMEB) on CH_4 hydrate formation. Despite having a four-carbon backbone, these compounds differ in their 3D geometries. The structures and stabilities of CH_4 hydrates containing each compound were analyzed using high-resolution powder diffraction, solid-state ^{13}C NMR, and phase equilibrium measurements. The experimental results revealed that *c*23EB, 12EB, and 33DMEB act as sII/sH hydrate formers and thermodynamic promoters, whereas *t*23EB and DEB have opposite roles. These results were analyzed in relation to the 3D geometries and relative stabilities of various rotational isomers using DFT calculations. Hydrate structure was influenced by both the length and thickness of the added compounds. Moreover, an appropriate level of (not excessive) hydrophilicity induced by an oxirane group appeared to enhance the thermodynamic stability of the hydrates. This study provides insights into how the chemical nature of additives influences the structure and stability of clathrate hydrates.

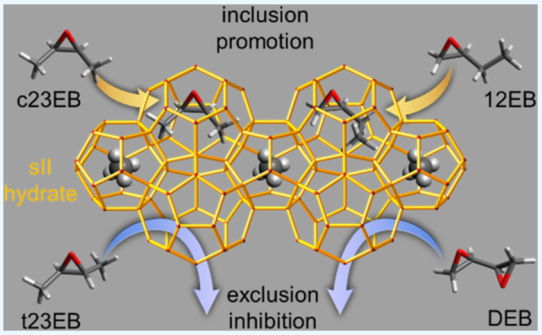

1. INTRODUCTION

Clathrate hydrates are host−guest inclusion compounds comprising hydrogen-bonded host frameworks and guest molecules. Although various semiclathrate hydrates containing ionic guest molecules have been studied, clathrate hydrates containing nonionic guest molecules typically exhibit three crystal structures. The simplest hydrate structure is structure I (sI), consists of 46 water molecules forming 2 pentagonal dodecahedral (5^{12}, sI-S) and 6 tetracaidecahedral ($5^{12}6^2$, sI-L) cages. This structure primarily accommodates small gas molecules, such as CH_4, CO_2, or Xe. When larger molecules are introduced, the hydrate structures transition to structure II (sII) or structure H (sH). The cubic sII structure comprises 136 water molecules forming 16 pentagonal dodecahedral (sII-S) and 8 hexakaidecahedral ($5^{12}6^4$, sII-L) cages. On the other hand, the hexagonal sH structure consists of 34 water molecules forming 3 pentagonal dodecahedral (sH-S), 2 irregular dodecahedral ($4^35^66^3$, sH-M), and 1 icosahedron ($5^{12}6^8$) cages. Relatively larger molecules occupy sII-L or sH-L cages, and these are referred to as large guest molecules (LGMs). These LGMs are also simply called "sII or sH formers". Certain LGMs that can independently form hydrates without any gaseous components (help gas) are called simple hydrate formers.

Numerous organic compounds can act as hydrate formers and are not limited to hydrocarbons. Diverse sII and sH formers contain various functional groups have been reported thus far, including hydroxyl,[1−8] ether,[9−17] ketone,[10,13,18−23] amine,[24−29] nitro,[30,31] and others.[32−36] The ability of a compound to act as a hydrate former and the specific hydrate structure it forms primarily depends on its size, although other factors also influence it. For example, diisopropyl amine is an sH former, whereas 2,4-dimethylpentane and diisopropyl ether are not, despite being isoelectric and exhibiting similar structures and size. Similarly, diethyl amine is an sH former, whereas *n*-pentane and diethyl ether are not.[27] Additionally, Lee et al.[37] proposed that when combined with 2,2-dimethylbutane (22DMB), *n*-pentane or *n*-hexane can enter the sH-L cage, despite lacking the ability to form sH hydrates. Furthermore, although methylcyclopentane is a representative sH former, cyclopentanol (with a methyl group substituted with a hydroxyl group) and cyclopentanemethanol (with an additional hydroxyl group on the methyl group) act as sII formers.[7,8]

However, no linear alkanes with a five-carbon backbone, including *n*-pentane, have been identified as sII formers thus far. In contrast, linear alkanes with a four-carbon backbone can form sH or sII hydrates in the presence of a help gas. For example, 2-methylbutane, 22DMB, 2,3-dimethylbutane, and 2,2,3-trime-

Received: August 10, 2023
Revised: October 20, 2023
Accepted: October 25, 2023
Published: November 9, 2023

https://doi.org/10.1021/acsomega.3c05901
ACS Omega 2023, 8, 43920−43929

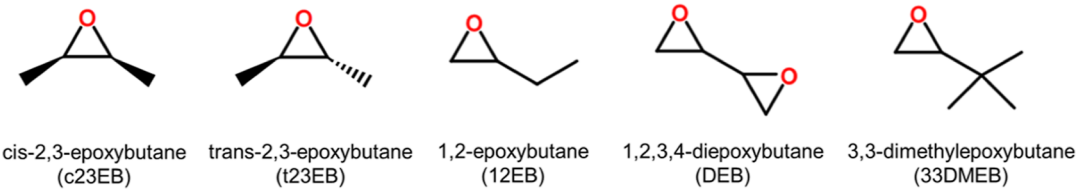

Figure 1. Structures of the five oxirane compounds investigated in this study.

Table 1. Chemicals Used in the Study

IUPAC name (common name)	abbreviation	CAS no	MW	supplier	product no	purity
cis-2,3-dimethyloxirane	*c*23EB	1758-33-4	72.11	Thermo Scientific	30787	97%
trans-2,3-dimethyloxirane	*t*23EB	21490-63-1	72.11	Thermo Scientific	B22005	97%
2-ethyloxirane	12EB	106-88-7	72.11	Merck	109975	99%
2-(oxiran-2-yl)oxirane	DEB	1464-53-5	86.09	Merck	202533	97%
2-*tert*-butyloxirane	33DMEB	2245-30-9	100.16	Thermo Scientific	L06951	95%
water	H_2O	7732-18-5	18.02	Merck	115333	LC−MS
methane	CH_4	74-82-8	16.04	Daesung Gas		99.95%

thylbutane are known to form sH hydrates.[38,39] Whereas, *n*-butane is an sII former, despite the anti-*n*-butane being too large to enter the sII-L cage. Experimental evidence has revealed that a conformational change in the gauche-*n*-butane occurs during hydrate formation.[39−41] In support of this, Ripmeester and Ratcliffe (1990) reported that *cis*-2-butene serves as an sII former (with Xe), but *trans*-2-butene does not.[39] However, research on other aspects of butene is limited.

Meanwhile, alkanes containing an oxirane group (hereafter oxiranes) can also act as hydrate formers. Oxirane, a cyclic ether, is a three-membered ring comprising an oxygen atom and two carbon atoms. Ethylene oxide[9] and propylene oxide (PO)[10] were identified as simple sI and sII hydrate formers, respectively. Recently, various oxiranes, such as 1,2-epoxycyclopentane (12ECP),[15] 3,4-epoxytetrahydrofuran,[16] 1,2-epoxycyclohexane (12ECH),[16] and epoxyisobutane (EIB),[17] were additionally identified as sII hydrate formers and thermodynamic promoters. Among these, 12ECP and EIB are simple sII hydrate formers. In particular, 12ECP significantly increased the dissociation temperature of CH_4 hydrate by ∼23 K at any given pressure, demonstrating a superior promotion capacity compared to tetrahydrofuran or cyclopentane.[15] Potential applications of 12ECP hydrates for energy gas storage[42−44] and CO_2 capture[45] were also suggested.

However, limited research has been conducted on oxiranes with linear alkane backbones. Oxiranes with a four-carbon backbone, similar to simple alkanes with four-carbon backbones, are expected to form sII or sH hydrates. However, because of the relatively hydrophilic nature of oxiranes, guest behavior, thermodynamic stability, and other properties of their hydrates may differ from those of simple alkane hydrates. Furthermore, exploring the conformational changes upon entrapping oxiranes in specific cages provides valuable insights into hydrate research. In light of these considerations, this study focused on (1) the ability to form hydrates based on molecular sizes and shapes of the oxirane compounds, (2) the molecular configurations of oxirane LGMs within the hydrate cages, and (3) the effect of oxirane groups on hydrate stability.

To achieve this, five commercially available oxiranes were selected: *cis*-2,3-dimethyloxirane, *trans*-2,3-dimethyloxirane, 2-ethyloxirane, 2-(oxiran-2-yl)oxirane, and 2-*tert*-butyloxirane, and their respective CH_4 hydrates were synthesized. For simplicity, this article uses their common names: *cis*-2,3-epoxybutane (*c*23EB); *trans*-2,3-epoxybutane (*t*23EB); 1,2-epoxybutane (12EB); 1,2,3,4-diepoxybutane (DEB); and 3,3-dimethylepoxybutane (33DMEB) (Figure 1 and Table 1). Although these compounds contain a four-carbon backbone, they differ in size and three-dimensional (3D) geometries. The physicochemical properties of the CH_4 hydrates containing each of the five compounds were analyzed using synchrotron high-resolution powder diffraction (HRPD), solid-state ^{13}C NMR, and phase equilibrium measurements. The experimental results were interpreted in relation to the 3D geometries and relative stabilities of various rotational isomers of each oxirane compound obtained using density functional theory (DFT) calculations.

2. EXPERIMENTAL SECTION

All chemicals listed in Table 1 were used as received without further purification. Figure 2 shows the experimental apparatus used to prepare the hydrate samples and measure the equilibrium P−T conditions. Each oxirane was mixed with water (x = 0.056 or 0.029) and 7−8 g of the mixture was charged

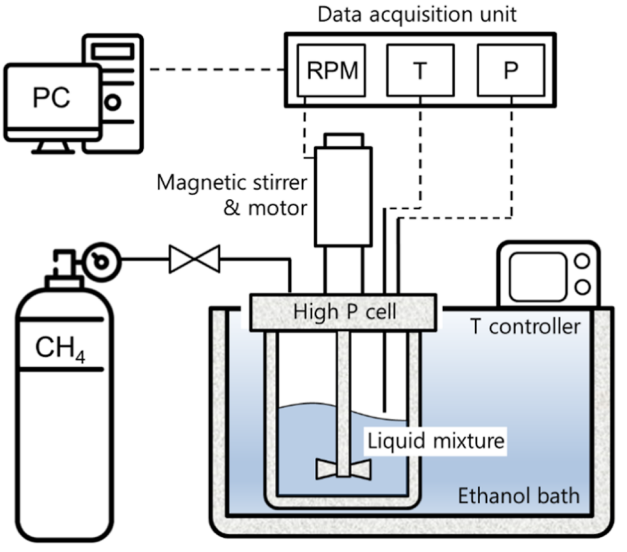

Figure 2. Experimental apparatus for sample preparation and equilibrium P−T measurement.

https://doi.org/10.1021/acsomega.3c05901
ACS Omega 2023, 8, 43920−43929

into a high-pressure resistance cell ($V \sim 100$ mL). The cell was pressurized with CH_4 to reach ~60 bar at ambient temperature (~290 K). The cell temperature decreased to 263 K at a rate of −1 K/h with continuous stirring at ~150 rpm. The solidified sample was quickly collected and finely ground into a powder ($d < 200$ μm) under a liquid nitrogen atmosphere for subsequent spectroscopic analyses.

To determine the four-phase equilibrium P−T conditions, the solid hydrate was prepared as described above, but the initial pressure was varied in the range of 25−85 bar. The cooled cell was slowly heated at a rate of +0.3 K/h while the stirring rate. The P and T inside the cell were measured by using a pressure transmitter (model A-10, WIKA, Germany) and a resistance temperature detector (Pt100-class B), respectively. P and T data were automatically recorded every minute until the temperature reached 293 K.

The crystal structures of the (oxirane + H_2O) samples were analyzed through powder X-ray diffraction (PXRD) measurements using Smartlab (RIGAKU) equipment at the KAIST Analysis Center for Research Advancement. The PXRD patterns were obtained in a range of $2\theta = 5.0-65.0°$ with a scan speed of 2° per 1 min, using an X-ray wavelength of $\lambda = 1.5418$ Å ($K_{\alpha1} = 1.5406$ Å and $K_{\alpha2} = 1.5444$ Å). For the (oxirane + CH_4) samples, a synchrotron HRPD instrument at the Pohang Accelerator Laboratory (beamline 9B) was used to obtain more precise lattice parameters. The HRPD patterns were obtained in a range of $2\theta = 5.0-125.0°$ with a scan speed of 0.01° per 0.7 s using an X-ray wavelength of $\lambda = 1.5425$ Å. PXRD and HRPD measurements were conducted at 150 K.

Solid-state ^{13}C NMR experiments were conducted using a Bruker AVANCE II 400 MHz NMR equipment at the Korea Basic Science Institute (Seoul Western Center). ^{13}C high-power decoupling/magic-angle spinning (MAS) NMR spectra were acquired by using a 4 mm OD zirconia rotor with a MAS rate of 5 kHz at 210 K. A pulse length (p1) of 1.6 μs and repetition delay time (d1) of 3 s were applied. The static ^{13}C signal of tetramethylsilane at room temperature was used as the reference (0 ppm).

The optimized geometries of each molecule were calculated using the Gaussian 03 software[46] with the B3LYP model at the 6-311++G (d, p) basis level. Torsional energy profiles were obtained by calculating the energies of the rotational isomers with different dihedral angles at 10° intervals. For 12EB, the ^{13}C NMR shielding constants of each optimized conformer were calculated using the gauge-including-atomic-orbital (GIAO) method at B3LYP/6-311++G (2d, p). The chemical shifts were calculated based on the chemical shielding of tetramethylsilane, which was used as the reference (0 ppm).

3. RESULTS AND DISCUSSION

The van der Waals (vdW) radii of oxygen and hydrogen atoms are 1.58 and 1.10 Å, respectively.[47] However, an oxirane group is expected to have a slightly smaller volume than an ethyl group, as it contains one oxygen atom instead of the two hydrogen atoms in the latter. According to the volume calculation, in fact, ethylene oxide and ethane exhibited almost identical molar volumes of 40.1 and 41.2 cm^3/mol, respectively (Figure 3a,b). Consequently, in light of molecular volume, *c*23EB, *t*23EB, 12EB, and DEB were anticipated to behave similarly to *n*-butane, forming sII hydrates. On the other hand, 33DMEB was expected to form an sH hydrate, similar to 22DMB. Therefore, the samples were prepared with the sII composition ($x = 0.056$) and sH composition ($x = 0.029$) for (*c*23EB/*t*23EB/12EB/DEB) and 33DMEB, respectively.

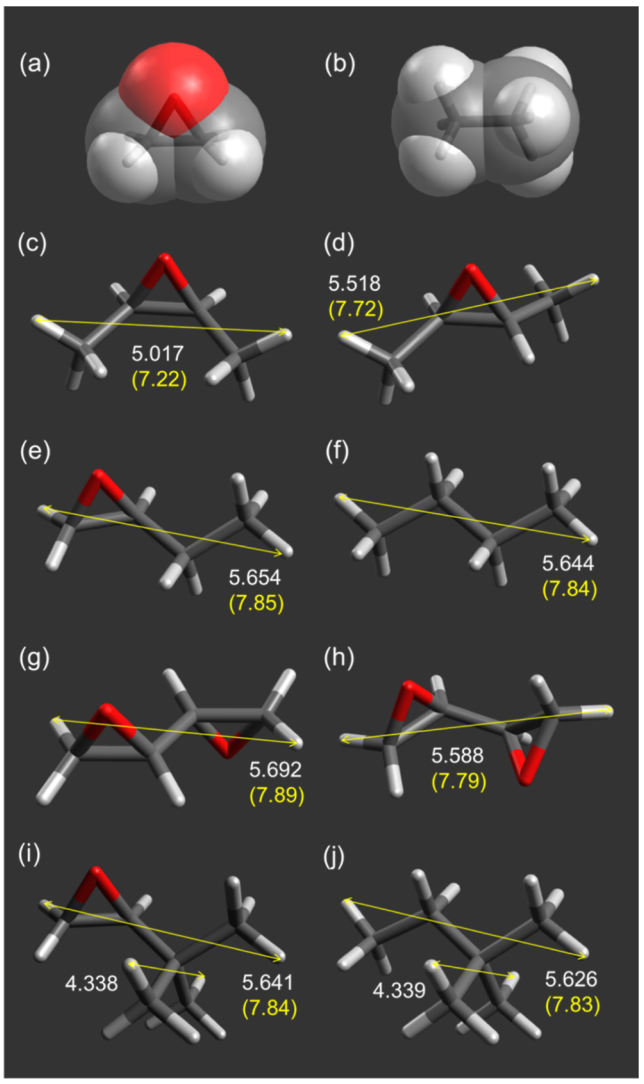

Figure 3. vdW surfaces of (a) ethylene oxide and (b) ethane molecules. The most stable conformers of (c) *c*23EB, (d) *t*23EB, (e) 12EB, (f) *n*-butane, (g) meso-DEB, (h) (S,S)-DEB, (i) 33DMEB, and (j) 22DMB. The center-to-center and vdW distances are given in Å.

Figure 3 also shows the optimized geometries of (c) *c*23EB, (d) *t*23EB, (e) 12EB, (f) *n*-butane, (g) meso-DEB, (h) (S, S)-DEB, (i) 33DMEB, and (j) 22DMB, all exhibiting the lowest energies. The geometries of all the oxirane rings are almost identical: (1) 61.5° of the COC bond angle, (2) 1.435 Å of the CO bond, (3) 1.469 Å of the CC bond, (4) 115.3° of HCH bond angle, and (5) 125.7° of CCC bond angle. Figure 5 also shows the longest center-to-center and vdW distances (i.e., end-to-end distances). Because the vdW radius of a hydrogen atom is 1.10 Å,[47] the vdW distances (d_{vdW}) were obtained by adding 2.20 Å to the center-to-center distances.

Figure 4 shows the HRPD patterns of CH_4 hydrates containing (a) *c*23EB, (b) *t*23EB, (c) 12EB, and (d) DEB with a stoichiometric composition ($x = 0.056$) of the sII hydrate. The red dots and black curves indicate the measured signals and profiles calculated using whole−pattern profile matching methods in the FullProf software,[48] respectively. The (*c*23EB + CH_4) and (12EB + CH_4) hydrates were identified as sII-type ($Fd\bar{3}m$) with lattice parameters of $a = 17.274$ and 17.249 Å,

https://doi.org/10.1021/acsomega.3c05901
ACS Omega 2023, 8, 43920−43929

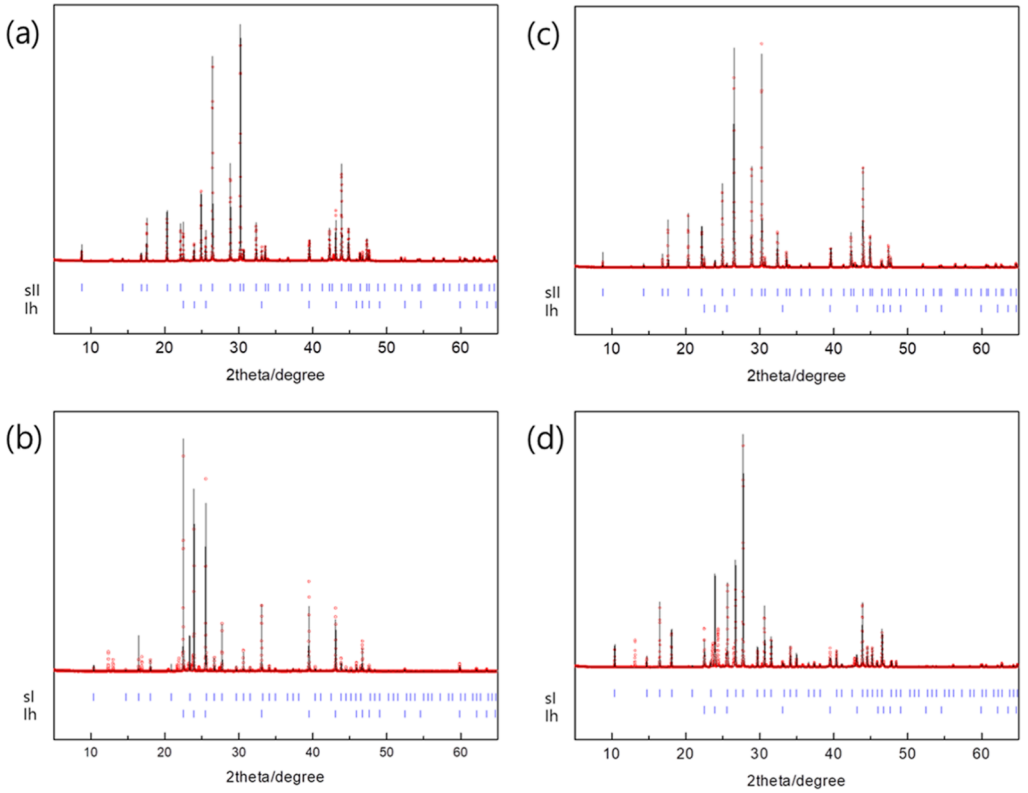

Figure 4. HRPD patterns (at 150 K) of the CH_4 hydrates containing (a) *c*23EB (R_e = 9.23%, R_{wp} = 30.4% and χ^2 = 10.9), (b) *t*23EB (R_e = 10.5%, R_{wp} = 73.6% and χ^2 = 49.4), (c) 12EB (R_e = 9.39%, R_{wp} = 32.2% and χ^2 = 11.8), and (d) DEB (R_e = 9.42%, R_{wp} = 77.4% and χ^2 = 67.6). The relatively high χ^2 values in the *t*23EB and DEB samples may be due to unmatched peaks from pure solid oxiranes.

respectively. These values are similar to that of (*n*-butane + CH_4) hydrate (*a* = 17.230 Å at 138 K).[41] In contrast, the (*t*23EB + CH_4) and (DEB + CH_4) hydrates were sI-type (*Pm*3*n*) with *a* = 11.879 Å and *a* = 11.877 Å, respectively, which are nearly identical to the reported value of simple CH_4 hydrate (*a* = 11.869 Å at 150 K).[49] On the other hand, Figure S1 shows that none of the four oxirane compounds can form simple hydrates.

Figure 5 shows the solid-state ^{13}C NMR spectra measured at 210 K. The (12EB + CH_4) and (*c*23EB + CH_4) hydrates exhibited two peaks near −4.6 and −8.2 ppm, attributed to the CH_4 molecules entrapped in sII-S and sII-L cages, respectively. Given that the area ratios (sII-L:sII-S) for both 12EB and *c*23EB hydrates were quite small (1:20), most of the sII-L cages of the hydrates were occupied by 12EB and *c*23EB molecules. In contrast, the (*t*23EB + CH_4) and (DEB + CH_4) hydrates exhibited two peaks near −4.3 and −6.7 ppm, indicative of the CH_4 molecules in sI-S and sI-L cages, respectively. Figure S2 indicates that even when the sH composition (*x* = 0.029) was employed, both *t*23EB and DEB formed sI hydrates only. Therefore, it is apparent that both *t*23EB and DEB did not participate in the formation of double hydrates and were excluded from the sI phase.

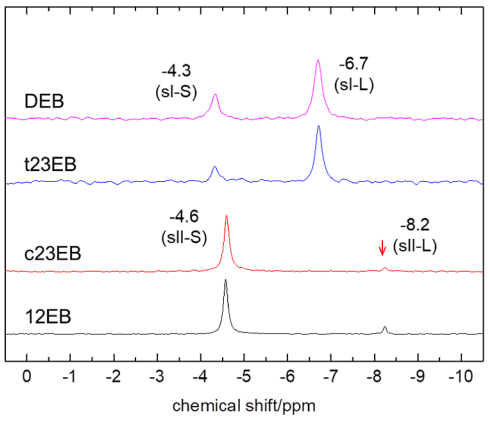

Figure 5. Solid-state ^{13}C NMR spectra (at 210 K) of the CH_4 hydrates containing 12EB (black), *c*23EB (red), *t*23EB (blue), and DEB (magenta).

On the other hand, Figure 6a indicates that the (33DMEB + CH_4) hydrate is sH-type (*P*6/*mmm*) with lattice parameters of a = 12.210 and c = 10.032 Å. These values are similar to those of (22DMB + CH_4) hydrate, *a* = 12.199 Å and *c* = 10.020 Å.[50] In Figure 5b, two peaks at −4.5 and −4.9 ppm are observed, attributed to CH_4 in sH-S and sH-M cages, respectively. The area ratio was 1.36:1, consistent with the theoretical ratio of 1.5:1. No peak corresponding to CH_4 in sH-L cage[51] was detected, indicating that the sH-L cages are exclusively occupied by 33DMEB. Figure S3 demonstrates that 33DMEB fails to form a simple hydrate, and even with an increased composition (up to *x* = 0.056), it does not form any structures other than sH.

Table 2 lists the CH_4 occupancy ratios, which were determined based on the peak areas obtained from the ^{13}C NMR spectra. For sII hydrates, the method suggested in previous studies was used.[15,17] For sH hydrates, similarly assuming that the sH-L cage is completely occupied by oxirane molecules ($\theta_{L,LGM}$ = 1), $\theta_{S,CH4}$ and $\theta_{M,CH4}$ can be calculated as follows.

https://doi.org/10.1021/acsomega.3c05901
ACS Omega 2023, 8, 43920−43929

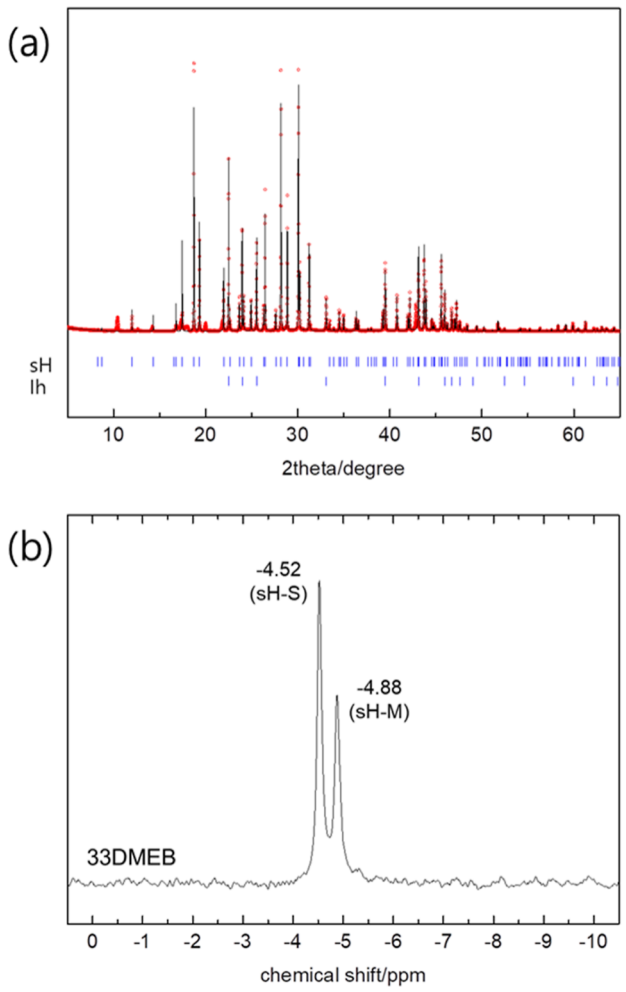

Figure 6. (a) HRPD pattern (at 150 K) (R_e = 9.99%, R_{wp} = 45.5% and χ^2 = 20.8), and (b) solid-state ^{13}C NMR spectrum (at 210 K) of the (33DMEB + CH_4) hydrate.

Table 2. CH_4 Occupancy Ratios

		CH_4 occupancy			
LGM	structure	θ_S	θ_M	θ_L	CH_4 storage[a] mmol CH_4/mol H_2O
c2EB	sII	0.86		0.05	101 (86%)
12EB	sII	0.61		0.06	72 (61%)
33DMEB	sH	0.74	0.82	0	113 (77%)

[a]These values were calculated excluding the CH_4 in the largest cages. The values within the parentheses represent the ratio to the theoretical CH_4 storage capacity.

$$\theta_{S,CH4} = \frac{A_{S,CH4}/3}{A_{L,LGM}/n_{EC}}$$

$$\theta_{M,CH4} = \frac{A_{M,CH4}/2}{A_{L,LGM}/n_{EC}}$$

where $A_{i,j}$ is the area of the ^{13}C NMR peak from molecule j in cage type i, and n_{EC} is the number of equivalent carbon atoms in an LGM molecule. The $\theta_{S,CH4}$ values of (c23EB/12EB + CH_4) hydrates are similar to that of (n-butane + CH_4) hydrate (~0.80).[52] The $\theta_{S,CH4}$ and $\theta_{S,CH4}$ of (33DMEB + CH_4) hydrate are also similar to those of (22DMB + CH_4) hydrate.[53,54] Therefore, it can be inferred that the effect of the oxirane group on the CH_4 occupancy is not significantly pronounced.

Here, it is necessary to understand the effects of oxiranes on CH_4 hydrates. Figure 7 compares the torsional energy profiles of 22DMB and 33DMEB. The energy profile of 22DMB is consistent with the previously reported profile.[55] The torsional energy barrier of 33DMEB (15.3 kJ/mol) is smaller than that of 22DMB (19.3 kJ/mol). Figure 7 indicates that 22DMB and 33DMEB exist as single conformers. Additionally, as shown in Figure 3i,j, the overall dimensions of the most stable conformers of 33DMEB and 22DMB are nearly identical. Therefore, similar to 22DMB, 33DMEB can be accommodated in an sH-L cage, forming an sH hydrate with similar unit cell parameters.

Next, c23EB and t23EB have entirely different effects on hydrate formation. c23EB cannot be converted into t23EB, and vice versa, owing to an oxirane ring at the center of the molecule. Furthermore, both c23EB and t23EB lack other stable conformers owing to the rigid nature of the oxirane ring. As described above, c23EB form a double hydrate (sII) with CH_4, whereas t23EB fail to form an sII hydrate. This observation suggests that c23EB has an appropriate shape and size (d_{vdW} ~ 7.22 Å) to fit inside an sII-L cage. Conversely, a molecule equal to or larger than t23EB (d_{vdW} ~ 7.72 Å) is too large to fit inside an sII-L cage. Moreover, despite its similar length to 33DMEB or 22DMB, t23EB does not form an sH hydrate. As Ripmeester and Ratcliffe pointed out,[39] the linear shape of a guest molecule cannot effectively establish vdW contact with water molecules comprising the sH-L cage.

Figure 3e shows the most stable conformer of 12EB, anti-12EB. Its size (d_{vdW} ~ 7.85 Å) is comparable to that of DMEB or t23EB. Similar to t23EB, anti-12EB is too long to form an sII hydrate and too narrow to form an sH hydrate. However, 12EB clearly forms the (12EB + CH_4) double hydrate and occupies the sII-L cage (Figures 4 and 5). Figure 8 compares the torsional energy profiles of n-butane and 12EB. The energy profile of n-butane (Figure 8a) consistently reflects the previously reported values.[56] In 12EB, there are two gauche conformers with dihedral angles of −24° (II) and 96° (III). Their sizes are similar (d_{vdW} ~ 7.4 Å) and smaller than that of anti-12EB (I) and similar to that of c23EB. Compared to the anti-12EB (I) with a dihedral angle of 145°, these conformers (II) and (III) have relative energies of +4.1 and +0.84 kJ/mol, respectively (Figure 8b). The transformation must overcome energy barriers of 14.4 (I → II) or 11.4 kJ/mol (I → III). Meanwhile, based on previous studies, only gauche-n-butane can enter the sII-L cage.[39−41] Considering that the energy barrier for the anti−to−gauche transition (I → II) of n-butane is 13.5 kJ/mol (Figure 8a), it can be inferred that this level of energy barrier is sufficiently surmountable during hydrate formation. Accordingly, the anti-12EB can also be readily transformed into gauche-12EBs (I → II or I → III).

Figure 9 shows the solid-state ^{13}C NMR spectra of the (12EB + H_2O), (12EB + CH_4), and (12EB + CO_2) samples, and Table 3 lists the corresponding chemical shifts (δ_{obs}). For (12EB + H_2O), four distinct peaks were observed near 53, 46, 26, and 10 ppm, corresponding to C2, C1, C3, and C4 of 12EB, respectively. When 12EB enters an sII-L cage to form the (12EB + CH_4) or (12EB + CO_2) hydrate, these four peaks shifted toward the upfield region by −2.0 to −3.4 ppm. Table 3 also lists the chemical shifts calculated using the GIAO method (δ_{calc}). Although the calculated values do not exactly match the observed values, it is clearly shown that (1) the anti-(I) and gauche-(III) exhibit similar chemical shifts; and (2) the gauche-(II) exhibits upfield-shifted values by −2 to −6 ppm. This

https://doi.org/10.1021/acsomega.3c05901
ACS Omega 2023, 8, 43920−43929

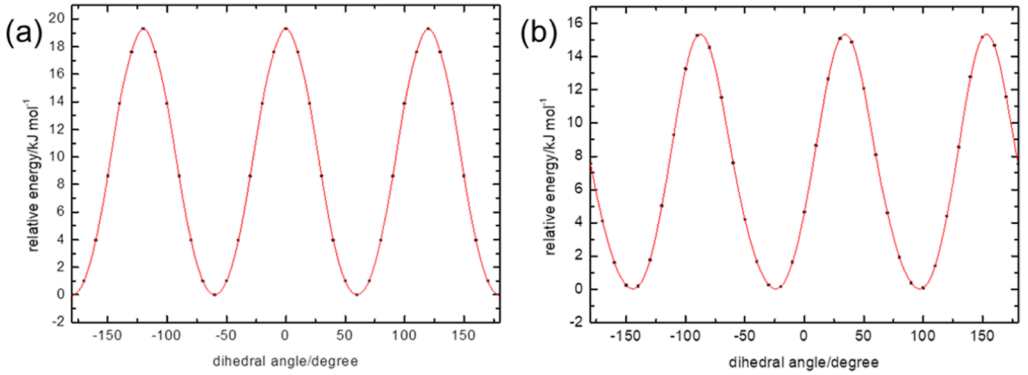

Figure 7. Torsional energy profiles of (a) 22DMB and (b) 33DMEB.

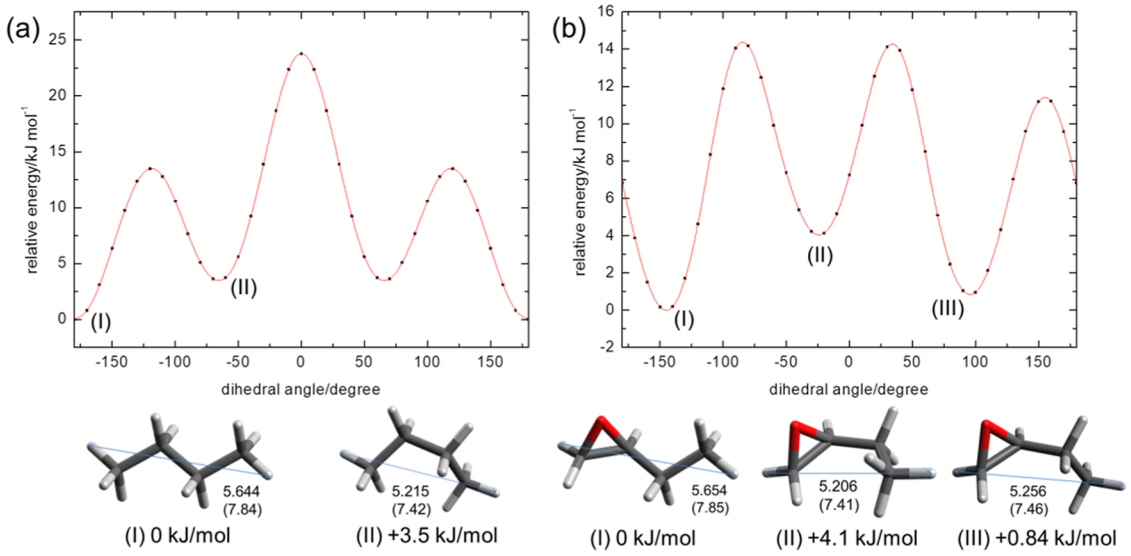

Figure 8. Torsional energy profiles of (a) *n*-butane and (b) 12EB.

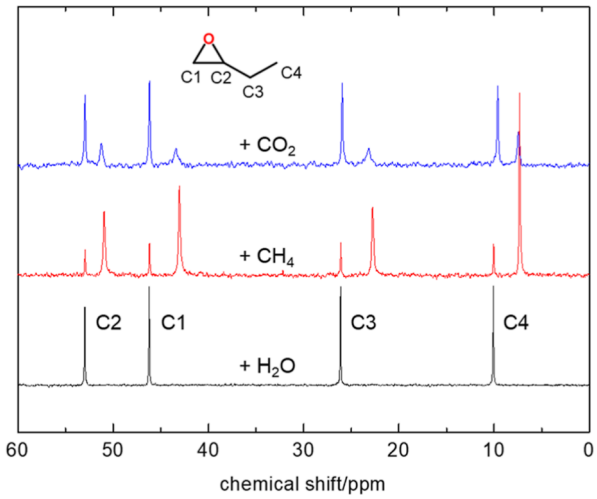

Figure 9. Solid-state ^{13}C NMR spectra (at 210 K) of the (12EB + H_2O) (black), (12EB + CH_4) (red), and (12EB + CO_2) (blue) samples.

suggests that an 12EB molecule in an sII-L cage prefers the gauche-(II) conformation over the gauche-(III) conformation. It is somewhat unexpected because gauche-(II) is energetically higher than gauche-(III). However, it should be noted that the gauche-(II) conformation bears a significant resemblance to *cis*-12EB. This "*cis*-like" geometry can effectively fill the nearly spherical sII-L cage, thereby allowing for sufficient stabilization.

Table 3. Experimentally Measured and Calculated Chemical Shifts of 12EB

	type	C2	C1	C3	C4
δ_{obs} (ppm)	+H_2O	52.97	46.21	26.13	10.08
	+CH_4[a]	50.95 (−2.02)	43.05 (−3.16)	22.77 (−3.36)	7.33 (−2.75)
δ_{calc} (ppm)	anti (I)	56.66	48.79	31.20	12.26
	gauche (II)[b]	54.98 (−1.68)	44.14 (−4.65)	25.94 (−5.26)	5.85 (−6.41)
	gauche (III)[b]	56.78 (+0.12)	49.16 (+0.37)	30.70 (−0.50)	10.66 (−1.60)

[a]The differences in chemical shift values compared to (12EB + H_2O) are indicated in parentheses. [b]The differences in chemical shift values compared to anti-12EB are indicated in parentheses.

Meanwhile, owing to the presence of two chiral centers, DEB exists as three different stereoisomers: (R, S), (R, R), and (S, S). The (R, S) represents the meso compound, whereas (R, R) and (S, S) have the same molecular size and chemical properties. Figure 3g,h show the most stable conformers of meso-DEB and (S, S)-DEB, respectively. Given their large sizes ($d_{vdW} \geq 7.8$ Å) and narrow shapes, neither will effectively fit inside an sII-L or sH-L cage. However, similar to 12EB, both meso- and (S, S)-

https://doi.org/10.1021/acsomega.3c05901
ACS Omega 2023, 8, 43920−43929

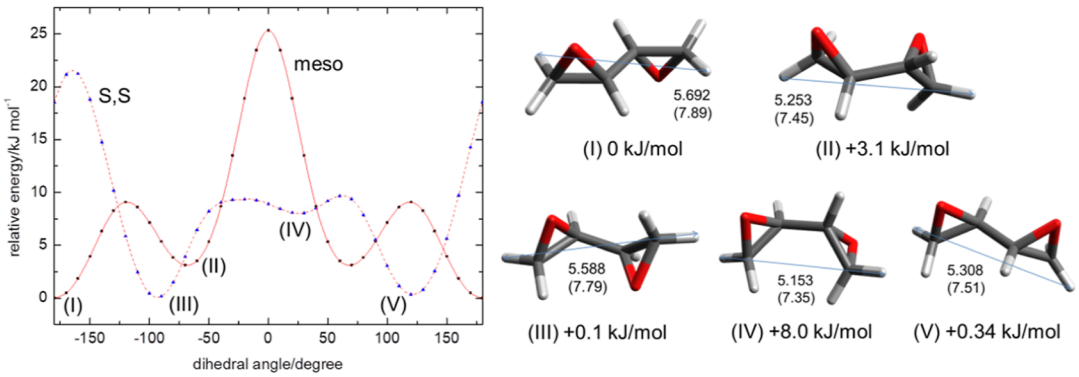

Figure 10. Torsional energy profiles of meso-DEB and (S, S)-DEB. The relative energies are based on the value of the most stable conformer, meso-anti-DEB (I).

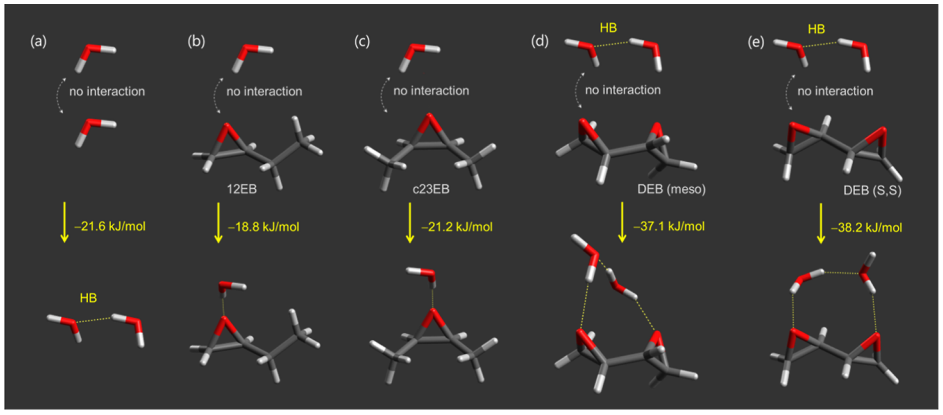

Figure 11. Hydrogen bonds between molecules: (a) two H_2O, (b) H_2O and 12EB, (c) H_2O and *c*23EB, (d) two H_2O and meso-DEB (II), and (e) two H_2O and (S, S)-DEB (V).

DEB have rotational isomers with smaller sizes. Also, their rotational energy barriers are lower than those of 12EB (Figure 10). For instance, meso-anti-DEB (I) can be transformed into meso-gauche-DEB (II) by overcoming an energy barrier of 9.1 kJ/mol. Similarly, (S, S)-anti-DEB (III) can be transformed into the other conformations (IV and V) by overcoming the energy barriers of 9.4 kJ/mol (III → IV) and 9.7 kJ/mol (III → IV → V). The sizes of these conformers (II, IV, and V) are $d_{vdW} \sim 7.4-7.5$ Å, similar to that of gauche-12EB that occupies an sII-L cage. In particular, the relative energies for (II) and (V) are only +3.1 and +0.34 kJ/mol, respectively, indicating that both are also sufficiently stable compared to the most stable conformers, (I) and (III).

However, the HRPD and ^{13}C NMR results clearly demonstrated that DEB does not form either sII or sH hydrates. This could be attributed to the strong hydrogen bonds between DEB and the water molecules. Among the five oxiranes investigated, only DEB exhibited complete miscibility with water (at least up to $x = 0.056$), while the others exhibited limited miscibility and formed organic layers on top of the water. Figure 11 illustrates the hydrogen bonding energies between oxirane and water molecules. The hydrogen bonding energy between two water molecules was calculated to be 21.6 kJ/mol, which aligns well with the reported values of ∼23 kJ/mol.[57,58] 12EB and *c*23EB can form hydrogen bonds with water with energies of 18.8 and 21.2 kJ/mol, respectively, which are comparable to or slightly lower than water−water hydrogen bonding. However, due to the limited miscibility of 12EB and 23EB in water, only a small portion of them is likely to engage in such hydrogen bonding interactions. Therefore, when hydrates form from liquid mixtures, it may not be necessary to break many water−oxirane bonds.

In contrast, DEB can interact with at least two water molecules, providing a stabilization energy of ∼38 kJ/mol (19 kJ/mol per hydrogen bond). Furthermore, DEB readily mixes with water to form a homogeneous solution. Therefore, during the hydrate formation, it would be necessary to break all water−DEB bonds. However, because a water−oxirane interaction is similar to a water−water interaction, disrupting all water−DEB hydrogen bonds while achieving vdW interactions to form a host (water)−guest (DEB) structure would not yield an energy advantage. Accordingly, it can be concluded that even if a DEB molecule transforms into a size-appropriate (II) or (V) form, it is challenging for it to stabilize inside the cage because of the strong hydrogen bonds with two or more water molecules. Instead, the presence of a substantial amount of surrounding water molecules around the DEB could potentially inhibit hydrate formation. It should be noted that the results obtained from calculations involving only a limited number of molecules may not perfectly align with the actual phenomena. Nonetheless, they provide a qualitative explanation that complements our understanding of the experimental results.

Figure 12 and Table S1 illustrate the equilibrium P−T conditions of CH_4 hydrates containing the five oxiranes. The data for the simple CH_4 hydrate are from Adisasmito et al.[59] At given pressures, the dissociation temperatures of the (33DMEB + CH_4) hydrate are 6−7 K higher than those of the simple CH_4 hydrate. Similarly, 12EB demonstrates a comparable promotion

https://doi.org/10.1021/acsomega.3c05901
ACS Omega 2023, 8, 43920−43929

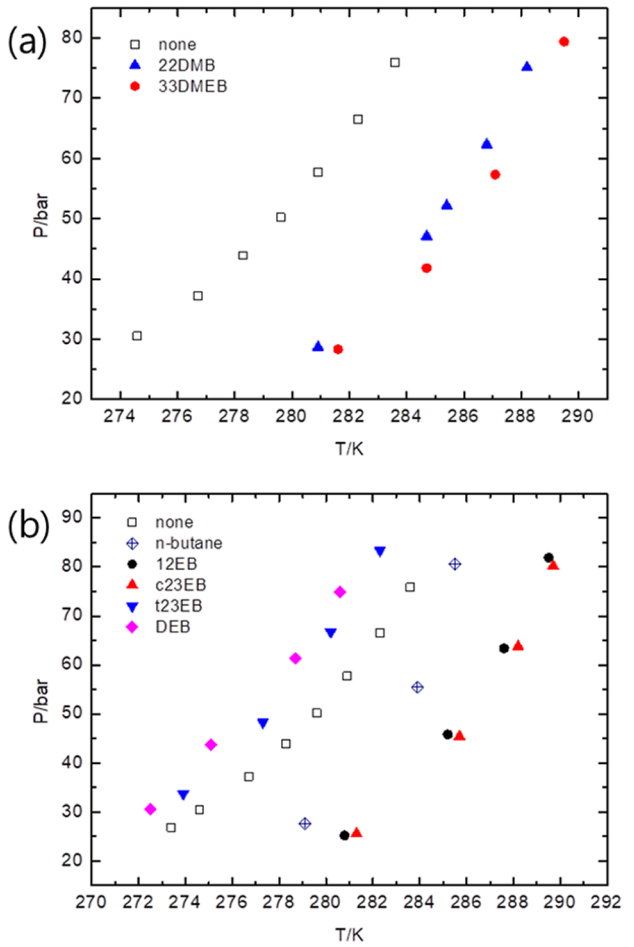

Figure 12. Equilibrium P−T conditions of the CH_4 hydrates (a) containing 33DMEB and 22DMB (x = 0.029); (b) containing 12EB, *c*23EB, *t*23EB, DEB (x = 0.056), and *n*-butane. The data for none (simple CH_4 hydrate),[59] 22DMB,[60,61] and *n*-butane (CH_4/*n*-butane = 94.5/5.5)[62] are from previous studies.

effect (+5 to 7 K) in the measured pressure range. The promotion capacity of *c*23EB is similar to, or slightly higher than, that of 12EB. As concluded above, 12EB adopts a "*cis*-like" geometry within the sII-L cage, closely resembling the geometry of *c*23EB. This similarity is likely one of the reasons behind the similar thermodynamic stability observed in (12EB + CH_4) and (*c*23EB + CH_4) hydrates. On the other hand, EIB, another isomer of 12EB and *c*23EB, exhibits a significantly higher promotion capacity (+15 K).[17] This is also partly because the EIB has a geometry that enables more effective filling of the nearly spherical sII-L cage.

Here, it should be also noted that both 33DMEB and 12EB/*c*23EB exhibited higher promotion capacities than 22DMB[60,61] and *n*-butane,[62] respectively, despite the similarity in molecular sizes and geometries. This trend has consistently been reported in other (oxirane + CH_4) vs (simple alkane + CH_4) systems, such as PO vs propane,[17] EIB vs *i*-butane,[17] 12ECP vs CP,[15] 12ECH vs cyclohexane.[16] The higher stability of oxirane hydrate is an intriguing finding. An appropriate hydrophilicity induced by an oxirane group appears to contribute to the additional stability, but further research is needed.

In contrast, *t*23EB exhibits an inhibitory effect, decreasing the dissociation temperature by nearly 2 K. Similarly, DEB also demonstrates an inhibition effect, but a larger depression in the dissociation temperature (−3 K) was observed. This strong inhibition corroborates the computational findings of the strong and multiple hydrogen bonds described above (Figure 11). Additionally, although only two examples are available, oxiranes that do not form hydrates can be considered as inhibitors of hydrate formation through their interaction with water. The effects of oxiranes are summarized in Figure 13. Considering the contrasting effects of oxiranes, more sophisticated and thorough studies of the unique interaction mechanisms of the oxirane group and its associated effects should be conducted.

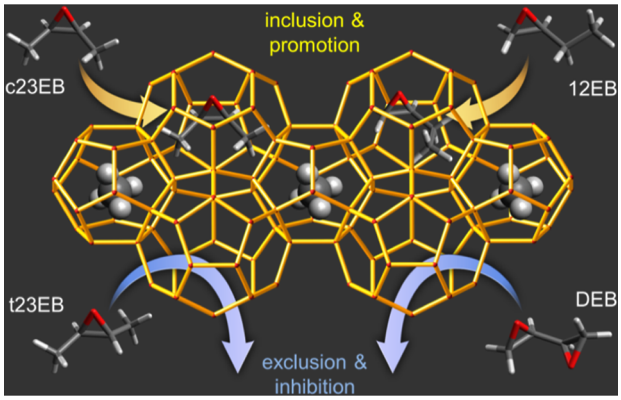

Figure 13. Schematic of CH_4 hydrate formation with four oxirane compounds.

4. CONCLUSIONS

This study investigates the effects of five oxirane compounds with a four-carbon backbone on the structure and stability of CH_4 hydrates. Specifically, *c*23EB, 12EB, and 33DMEB acted as sII/sH formers and thermodynamic promoters, whereas *t*23EB and DEB played opposite roles. The experimental results were analyzed in relation to the 3D geometries and relative stabilities of various rotational isomers of each oxirane compound by using DFT calculations. Interestingly, within the sII-L cage, 12EB appears to adopt a *cis*-like conformation rather than a more stable gauche conformation. However, because these geometry and energy calculations were performed without considering additional conformational changes upon interaction with water molecules, further studies should be conducted to explore the actual conformations of the guests inside the sII/sH-L cages. Alkanes with hydrophilic oxirane groups exhibited higher promotion capacities than those of structurally similar simple alkanes. This suggests that the appropriate hydrophilicity of a hydrate former enhances the thermodynamic stability of the hydrates. However, excessive hydrophilicity, as observed in the case of DEB, inhibits hydrate formation due to strong and multiple hydrogen bonds with water molecules. The author believes that this study enhances our understanding of how the geometry and hydrophilicity of the additives influence the structure and stability of clathrate hydrates.

■ ASSOCIATED CONTENT

Supporting Information

The Supporting Information is available free of charge at https://pubs.acs.org/doi/10.1021/acsomega.3c05901.

PXRD patterns of (*c*23EB/*t*23EB/12EB/DEB/33DMEB + H_2O) samples, ^{13}C NMR spectra of (*t*23EB/DEB/

https://doi.org/10.1021/acsomega.3c05901
ACS Omega 2023, 8, 43920−43929

33DMEB + CH_4) samples, and equilibrium P−T values (PDF)

AUTHOR INFORMATION

Corresponding Author

Jiwoong Seol − *Faculty of Liberal Education, Seoul National University, Gwanak-gu, Seoul 08826, Republic of Korea;* orcid.org/0000-0002-1832-4113; Email: seoljiwoong@snu.ac.kr

Complete contact information is available at: https://pubs.acs.org/10.1021/acsomega.3c05901

Notes

The author declares no competing financial interest.

ACKNOWLEDGMENTS

This study was supported by the Basic Science Research Program of the National Research Foundation of Korea funded by the Ministry of Education (2017R1D1A1B03033000 and 2022R1I1A1A01068394). The PLS-II experiments were partially supported by MSICT and POSTECH. Solid-state NMR experiments were conducted using a Bruker AVANCE II 400 MHz NMR system at the KBSI Seoul Western Center.

REFERENCES

(1) Østergaard, K. K.; Tohidi, B.; Anderson, R.; Todd, A. C.; Danesh, A. Can 2-propanol form clathrate hydrates? *Ind. Eng. Chem. Res.* **2002**, *41*, 2064−2068.

(2) Chapoy, A.; Anderson, R.; Haghighi, H.; Edwards, T.; Tohidi, B. Can n-propanol form hydrates? *Ind. Eng. Chem. Res.* **2008**, *47*, 1689−1694.

(3) Yasuda, K.; Takeya, S.; Sakashita, M.; Yamawaki, H.; Ohmura, R. Binary ethanol-methane clathrate hydrate formation in the system CH_4-C_2H_5OH-H_2O: confirmation of structure II hydrate formation. *J. Phys. Chem. C* **2009**, *113*, 12598−12601.

(4) Anderson, R.; Chapoy, A. C.; Haghighi, H.; Tohidi, B. Binary ethanol-methane clathrate hydrate formationin the system CH_4-C_2H_5OH-H_2O: phase equilibria and compositional analyses. *J. Phys. Chem. C* **2009**, *113*, 12602−12607.

(5) Youn, Y.; Cha, M.; Lee, H. Spectroscopic observation of the hydroxy position in butanol hydrates and its effect on hydrate stability. *ChemPhysChem* **2015**, *16*, 2876−2881.

(6) Park, K. H.; Kim, D. H.; Cha, M. Spectroscopic observations of host−guest interactions occurring in (cyclobutanemethanol + methane) hydrate and their potential application to gas storage. *Chem. Eng. J.* **2021**, *421*, 127835.

(7) Park, K. H.; Kim, D. H.; Cha, M. Spectroscopic identifications of structure II hydrate with new large alcohol guest molecule (Cyclopentanemethanol). *Chem. Phys. Lett.* **2021**, *779*, 138869.

(8) Park, K. H.; Kim, D. H.; Cha, M. Structure identification of binary (cyclic alcohol guests + methane) clathrate hydrates using Rietveld analysis with the direct space method. *Chem. Phys. Lett.* **2022**, *806*, 140054.

(9) McMullan, R. K.; Jeffrey, G. A. Polyhedral Clathrate Hydrates. IX. Structure of Ethylene Oxide Hydrate. *J. Chem. Phys.* **1965**, *42*, 2725−2732.

(10) Sargent, D. F.; Calvert, L. D. Crystallographic data for some new type II clathrate hydrates. *J. Phys. Chem.* **1966**, *70*, 2689−2691.

(11) Gough, S. R.; Davidson, D. W. Composition of Tetrahydrofuran Hydrate and the Effect of Pressure on the Decomposition. *J. Chem.* **1971**, *49*, 2691−2699.

(12) Miller, S. L.; Gough, S. R.; Davidson, D. W. Two clathrate hydrates of dimethyl ether. *J. Phys. Chem.* **1977**, *81*, 2154−2157.

(13) Kozaki, T.; Taguch, T.; Takeya, S.; Ohmura, R. Phase equilibrium for structure H hydrates formed with methane plus cycloheptane, cycloheptanone, or oxacycloheptane. *J. Chem. Eng. Data* **2010**, *55*, 3059−2062. (ether & ketone)

(14) Seo, D.; Moon, S.; Lee, Y.; Hong, S.; Lee, S.; Park, Y. Investigation of tuning behavior of trimethylene oxide hydrate with guest methane molecule and its critical guest concentration. *Chem. Eng. J.* **2020**, *389*, 123582.

(15) Seol, J.; Park, J.; Shin, W. Epoxycyclopentane hydrate for sustainable hydrate-based energy storage: notable improvements in thermodynamic condition and storage capacity. *Chem. Commun.* **2020**, *56*, 8368−8371.

(16) Seol, J.; Shin, W.; Park, J. Oxabicyclic Guest Compounds as sII Promoters: Spectroscopic Investigation and Equilibrium Measurements. *Chem.* **2020**, *8*, 614.

(17) Seol, J. Methane storage in clathrate hydrates containing water-miscible oxirane promoters. *J. Energy Res.* **2022**, *46*, 3249−3259.

(18) Quist, A. S.; Frank, H. S. Ice VIII-an acetone hydrate? *J. Phys. Chem.* **1961**, *65*, 560−562.

(19) Ohmura, R.; Uchida, T.; Takeya, S.; Nagao, J.; Minagawa, H.; Ebinuma, T.; Narita, H. Clathrate hydrate formation in (methane +water+methylcyclohexanone) systems: the first phase equilibrium data. *J. Chem. Thermodyn.* **2003**, *35*, 2045−2054.

(20) Tezuka, K.; Shen, R.; Watanabe, T.; Takeya, S.; Alavi, S.; Ripmeester, J. A.; Ohmura, R. Synthesis and characterization of a structure H hydrate formed with carbon dioxide and 3,3-dimethyl-2-butanone. *Chem. Commun.* **2013**, *49*, 505−507.

(21) Juan, Y.-W.; Tang, M.; Chen, L.-J.; Lin, S.-T.; Chen, P.-C.; Chen, Y.-P. Measurements for the equilibrium conditions of methane hydrate in the presence of cyclopentanone or 4-hydroxy-4-methyl-2-pentanone additives. *Fluid Phase Equilib.* **2015**, *386*, 162−167.

(22) Kondo, Y.; Alavi, S.; Takeya, S.; Ohmura, R. Characterization of the clathrate hydrate formed with fluoromethane and pinacolone: the thermodynamic stability and volumetric behavior of the structure H binary hydrate. *J. Phys. Chem. B* **2021**, *125*, 328−337.

(23) Ahn, Y.-H.; Kang, H.; Cha, M.; Shin, K.; Lee, H. Thermodynamic Stability of Structure II Methyl Vinyl Ketone Binary Clathrate Hydrates and Effects of Secondary Guest Molecules on Large Guest Conformation. *ACS Omega* **2017**, *2*, 1601−1607.

(24) Shin, W.; Park, S.; Koh, D.-Y.; Seol, J.; Ro, H.; Lee, H. Water-soluble structure H clathrate hydrate formers. *J. Phys. Chem. C* **2011**, *115*, 18885−18889.

(25) Youn, Y.; Seol, J.; Cha, M.; Ahn, Y.-H.; Lee, H. Structural transition induced by CH4 enclathration and cage expansion with large guest molecules occurring in amine hydrate systems. *J. Chem. Eng. Data* **2014**, *59*, 2004−2012.

(26) Youn, Y.; Cha, M.; Lee, H. Structural transition of trimethylamine semi-hydrate by methane inclusion. *Fluid Phase Equilib.* **2016**, *413*, 123−128.

(27) Seol, J. Selective inclusion of secondary amine guests in sH hydrate systems. *J. Chem. Eng. Data* **2021**, *66*, 3335−3345.

(28) Park, K. H.; Kim, D. H.; Cha, M. Phase Equilibria and Spectroscopic Identification of Structure II Hydrates with New Hydrate-Forming Agents (Cyclopropylamine and Cyclopentylamine). *J. Phys. Chem. C* **2022**, *126*, 13585−13594.

(29) Lee, S.; Ok, Y.; Lee, Y.; Seo, D.; Moon, S.; Park, Y. Exploring the tuning patterns of cyclopentylamine hydrate for potential application of CH_4 storage. *J. Environ. Chem. Eng.* **2022**, *10*, 108402.

(30) Seol, J. Incorporating nitroalkane promoters in methane hydrates for stability and energy density. *Energy Fuels* **2022**, *36*, 11972−11978.

(31) Seol, J. Structural and thermodynamic investigations of nitroalkane + CH_4 hydrates with structure II and H. *J. Chem. Eng. Data* **2023**, *68* (6), 1441−1446.

(32) Choi, S.; Shin, K.; Lee, H. Structure transition and tuning pattern in the double (tetramethylammonium hydroxide + gaseous guests) clathrate hydrates. *J. Phys. Chem. B* **2007**, *111*, 10224−10230.

(33) Cha, M.; Kwon, M.; Youn, Y.; Shin, K.; Lee, H. Phase equilibria and spectroscopic identification of (2-methylpropane-2-peroxol + gaseous guests) hydrates. *J. Chem. Eng. Data* **2012**, *57*, 1128−1133.

(34) Cha, M.; Baek, S.; Lee, H.; Lee, J. W. Inclusion of thiophene as a co-guest in a structure II hydrate with methane gas. *RSC Adv.* **2014**, *4*, 26176−26180.
(35) Cha, M.; Baek, S.; Lee, W.; Shin, K.; Lee, J. W. Tuning behaviors of methane inclusion in isoxazole clathrate hydrates. *J. Chem. Eng. Data* **2015**, *60*, 278−283.
(36) Ahn, Y.-H.; Youn, Y.; Cha, M.; Lee, H. Spectroscopic and thermodynamic investigations of clathrate hydrates of methacrolein. *RSC Adv.* **2017**, *7*, 12359−12365.
(37) Lee, J.-W.; Lu, H.; Moudrakovski, I. L.; Ratcliffe, C. I.; Ripmeester, J. A. n-pentane and n-hexane as coguests in structure-H hydrates in mixtures of 2,2-dimethylbutane and methane. *Angew. Chem., Int. Ed.* **2006**, *45*, 2456−2459.
(38) Mehta, A. P.; Sloan, E. D., Jr. Structure H hydrate phase equilibria of paraffins, naphthenes, and olefins with methane. *J. Chem. Eng. Data* **1994**, *39*, 887−890.
(39) Ripmeester, J. A.; Ratcliffe, C. I. Xenon-129 NMR studies of clathrate hydrates: new guests for structure II and structure H. *J. Phys. Chem.* **1990**, *94*, 8773−8776.
(40) Subramanian, S.; Sloan, E. D. Jr. Trends in vibrational frequencies of guests trapped in clathrate hydrate cages. *J. Phys. Chem. B* **2002**, *106*, 4348−4355.
(41) Takeya, S.; Fujihisa, H.; Hachikubo, A.; Sakagami, H.; Gotoh, Y. Distribution of Butane in the Host Water Cage of Structure II Clathrate Hydrates. *Chem.—Eur. J.* **2014**, *20*, 17207−17213.
(42) Chen, S.; Wang, Y.; Lang, X.; Fan, S.; Li, G.. Phase equilibrium of hydrogen clathrate hydrates with propylene oxide and 1,2-epoxycyclopentane. *J. Chem. Eng. Data* **2023**, *68*, 1184−1190.
(43) Chen, S.; Wang, Y.; Lang, X.; Fan, S.; Li, G.. Rapid and high hydrogen storage in epoxycyclopentane hydrate at moderate pressure. *Energy* **2023**, *268*, 126638.
(44) Wu, W.; Hao, B.; Guo, Y.; Yang, J.; Du, M.; Zheng, Q.; Bai, Z. Application of monocyclic compounds as natural gas hydrate promoters: a review. *Chem. Eng. Res. Des.* **2023**, *190*, 66−90.
(45) Moon, S.; Lee, S.; Ahn, Y.-H.; Park, Y. Abnormal thermodynamic promotion and tuning behavior of epoxycyclopentane for its implication in CO_2 storage. *Chem. Eng. J.* **2021**, *425*, 130647.
(46) Frisch, M. J.; Trucks, G. W.; Schlegel, H. B.; Scuseria, G. E.; Robb, M. A.; Cheeseman, J. R.; Montgomery, J. A.; Vreven, T.; Kudin, K. N.; Burant, J. C.; Millam, J. M.; Iyengar, S. S.; Tomasi, J.; Barone, V.; Mennucci, B.; Cossi, M.; Scalmani, G.; Rega, N.; Petersson, G. A.; Nakatsuji, H.; Hada, M.; Ehara, M.; Toyota, K.; Fukuda, R.; Hasegawa, J.; Ishida, M.; Nakajima, T.; Honda, Y.; Kitao, O.; Nakai, H.; Klene, M.; Li, X.; Knox, J. E.; Hratchian, H. P.; Cross, J. B.; Adamo, C.; Jaramillo, J.; Gomperts, R.; Stratmann, R. E.; Yazyev, O.; Austin, A. J.; Cammi, R.; Pomelli, C.; Ochterski, J. W.; Ayala, P. Y.; Morokuma, K.; Voth, G. A.; Salvador, P.; Dannenberg, J. J.; Zakrzewski, V. G.; Dapprich, S.; Daniels, A. D.; Strain, M. C.; Farkas, O.; Malick, D. K.; Rabuck, A. D.; Raghavachari, K.; Foresman, J. B.; Ortiz, J. V.; Baboul, Q. A. G.; Clifford, S.; Cioslowski, J.; Stefanov, B. B.; Liu, G.; Liashenko, A.; Piskorz, P.; Komaromi, I.; Martin, R. L.; Fox, D. J.; Keith, T.; Al-Laham, M. A.; Peng, C. Y.; Nanayakkara, A.; Challacombe, M.; Gill, P. M. W.; Johnson, B.; Chen, W.; Wong, M. W.; Gonzalez, C.; Pople, J. A. *Gaussian 03*, Revision C.01; Gaussian, Inc., Wallingford, CT, 2004.
(47) Rowland, R. S.; Taylor, R. Intermolecular nonbonded contact distances in organic crystal structures: Comparison with distances expected from van der Waals radii. *J. Phys. Chem.* **1996**, *100*, 7384−7391.
(48) Rodriguez-Carvajal, J. Recent advances in magnetic structure determination by neutron powder diffraction. *Phys. B* **1993**, *192*, 55−69.
(49) Gutt, C.; Asmussen, B.; Press, W.; Johnson, M. R.; Handa, Y. P.; Tse, J. S. The structure of deuterated methane−hydrate. *Chem. Phys.* **2000**, *113*, 4713−4721.
(50) Murayama, K.; Takeya, S.; Alavi, S.; Ohmura, R. Anisotropic Lattice Expansion of Structure H Clathrate Hydrates Induced by Help Guest: Experiments and Molecular Dynamics Simulations. *J. Phys. Chem. C* **2014**, *118*, 21323−21330.
(51) Lee, Y.; Moon, S.; Seo, D.; Lee, S.; Park, Y. Hydrogen-bonded clathrate hydrate as tunable media for efficient methane storage. *J. Environ. Chem. Eng.* **2022**, *10*, 108473.
(52) Kida, M.; Sakagami, H.; Watanabe, M.; Jin, Y.; Takahashi, N.; Nagao, J. Structural properties of methane and butane mixed-gas hydrates. *Chem. Eng. Sci.* **2016**, *140*, 10−15.
(53) Seo, Y.-T.; Lee, H. ^{13}C NMR analysis and gas uptake measurements of pure and mixed gas hydrates: development of natural gas transport and storage method using gas hydrate. *Korean J. Chem. Eng.* **2003**, *20*, 1085−1091.
(54) Susilo, R.; Ripmeester, J. A.; Englezos, P. Characterization of gas hydrates with PXRD, DSC, NMR, and Raman spectroscopy. *Chem. Eng. Sci.* **2007**, *62*, 3930−3939.
(55) Tezuka, K.; Murayama, K.; Takeya, S.; Alavi, S.; Ohmura, R. Effect of guest size and conformation on crystal structure and stability of structure H clathrate hydrates: Experimental and molecular dynamics simulation studies. *J. Phys. Chem. C* **2013**, *117*, 10473−10482.
(56) Wiberg, K. B.; Murcko, M. A. Rotational barriers. 2. Energies of alkane rotamers. An examination of gauche interactions. *J. Am. Chem. Soc.* **1988**, *110*, 8029−8038.
(57) Suresh, S. J.; Naik, V. M. Hydrogen bond thermodynamic properties of water from dielectric constant data. *J. Chem. Phys.* **2000**, *113*, 9727−9732.
(58) Khan, A. A liquid water model: density variation from supercooled to superheated states, prediction of H-bonds, and temperature limits. *J. Phys. Chem. B* **2000**, *104*, 11268−11274.
(59) Adisasmito, S.; Frank, R. J.; Sloan, E. D. Jr. Hydrates of carbon dioxide and methane mixtures. *J. Chem. Eng. Data* **1991**, *36*, 68−71.
(60) Mohammadi, A. H.; Richon, D. Equilibrium data of neohexane + hydrogen sulfide and neohexane + methane clathrate hydrates. *J. Chem. Eng. Data* **2011**, *56*, 5094−5097.
(61) Thomas, M.; Behar, E. Structure H hydrate equilibria of methane and intermediate hydrocarbon molecules. In *Proceedings of 73rd Gas Processors Association Convention*; Gas Processors Association: New Orleans, LA, 1994, pp 100−107. March 7−9.
(62) Smith, C.; Pack, D.; Barifcani, A. Propane, n-butane and i-butane stabilization effects on methane gas hydrates. *J. Chem. Thermodyn.* **2017**, *115*, 293−301.

https://doi.org/10.1021/acsomega.3c05901
ACS Omega 2023, 8, 43920−43929